ADVANCED ENERGY MATERIALS

www.advenergymat.de

Twist and Degrade—Impact of Molecular Structure on the Photostability of Nonfullerene Acceptors and Their Photovoltaic Blends

*Joel Luke, Emily M. Speller, Andrew Wadsworth, Mark F. Wyatt, Stoichko Dimitrov, Harrison K. H. Lee, Zhe Li, Wing C. Tsoi, Iain McCulloch, Diego Bagnis, James R. Durrant, and Ji-Seon Kim**

Nonfullerene acceptors (NFAs) dominate organic photovoltaic (OPV) research due to their promising efficiencies and stabilities. However, there is very little investigation into the molecular processes of degradation, which is critical to guiding design of novel NFAs for long-lived, commercially viable OPVs. Here, the important role of molecular structure and conformation in NFA photostability in air is investigated by comparing structurally similar but conformationally different promising NFAs: planar O-IDTBR and nonplanar O-IDFBR. A three-phase degradation process is identified: i) initial photoinduced conformational change (i.e., torsion about the core–benzothiadiazole dihedral), induced by noncovalent interactions with environmental molecules, ii) followed by photo-oxidation and fragmentation, leading to chromophore bleaching and degradation product formation, and iii) finally complete chromophore bleaching. Initial conformational change is a critical prerequisite for further degradation, providing fundamental understanding of the relative stability of IDTBR and IDFBR, where the already twisted IDFBR is more prone to degradation. When blended with the donor polymer poly(3-hexylthiophene), both NFAs exhibit improved photostability while the photostability of the polymer itself is significantly reduced by the more miscible twisted NFA. The findings elucidate the important role of NFA molecular structure in photostability of OPV systems, and provide vital insights into molecular design rules for intrinsically photostable NFAs.

1. Introduction

Organic photovoltaics (OPVs) have received large amounts of interest in research and commercial development due to their potential for low-cost, solution-processable, flexible solar cells. Solution-processed OPV devices are based on an organic bulk heterojunction (BHJ) blend consisting of a conjugated donor polymer and a small molecule acceptor. Typically, the small molecules used have been fullerene derivatives such as [6,6]-phenyl-C-61-butyric acid methyl ester ($PC_{60}BM$), [6,6]-phenyl-C-71-butyric acid methyl ester ($PC_{70}BM$), and 1′,1″,4′,4″-tetrahydro-di[1,4]-methanonaphthaleno[5,6]fullerene-C_{60} (ICBA), achieving efficiencies of 11%[1,2] and lifetimes exceeding several years.[3]

However, progress in fullerene-based devices has stalled due to several intrinsic limitations of fullerene-based derivatives. An inability to tune the chemical structure inhibits morphological or energetic optimization, to the effect that progress in the field has mostly been driven by the design

J. Luke, Prof. J.-S. Kim
Department of Physics and Centre for Plastic Electronics
Imperial College London
London SW7 2AZ, UK
E-mail: ji-seon.kim@imperial.ac.uk

Dr. E. M. Speller, Dr. S. Dimitrov, Dr. H. K. H. Lee, Dr. W. C. Tsoi, Prof. J. R. Durrant
SPECIFIC IKC
College of Engineering
Swansea University
Bay Campus, Fabian Way, Swansea, Wales SA1 8EN, UK

Dr. A. Wadsworth, Prof. I. McCulloch, Prof. J. R. Durrant
Department of Chemistry and Centre for Plastic Electronics
Imperial College London
London SW7 2AY, UK

The ORCID identification number(s) for the author(s) of this article can be found under https://doi.org/10.1002/aenm.201803755.

Dr. M. F. Wyatt
EPSRC UK National Mass Spectrometry Facility (NMSF)
Swansea University Medical School
Singleton Park, Swansea SA2 8PP, UK

Dr. Z. Li
School of Engineering
Cardiff University
Cardiff, Wales CF24 3AA, UK

Prof. I. McCulloch
KSC King Abdullah University of Science and Technology
Thuwal 23955-6900, Saudi Arabia

Dr. D. Bagnis
Centro de Inovações
CSEM Brasil
Av. José Cândido da Silveira, 2000 Horto Florestal, Belo Horizonte, MG 31035-536, Brazil

DOI: 10.1002/aenm.201803755

and fine tuning of the donor polymers used within the blends.[4] Fullerenes are also poor absorbers possessing a wide band gap that limits their contribution to light harvesting across the entire solar spectrum. Stability issues are also common, with light-induced effects causing strong burn-in degradation,[5,6] poor thermal stability,[7–9] and photo-oxidation,[10,11] reducing the viability of using fullerene-based acceptors in commercial modules. Efforts have been made to address these issues and improvements in stability have been achieved but morphological and light-induced degradation effects still remain. In the last few years, nonfullerene acceptors (NFAs) have replaced fullerenes as the acceptor of choice and have already achieved high efficiencies (>13%)[12,13] and burn-in free devices.[14,15] Accompanied by reports of good compatibility with nonchlorinated solvents[16] and low thickness-dependent performance,[17] NFAs provide encouraging potential for commercial scale-up. However, the origin of these impressive stabilities is poorly understood, and there is still plenty of room for improvement, especially concerning their stability in air.

Due to the different classes of molecules used as NFAs, it is difficult to apply broad design rules. For example, it is known that there is a need to balance an acceptor's propensity to crystallize with its miscibility in the donor polymer, to achieve an optimal BHJ morphology. One approach, demonstrated by Hwang et al., is to disrupt the packing of naphthalene diimide (NDI) based dimers by increasing the torsion angle between the two units, leading to an improved morphology and better device performance.[18] Another approach to achieve an optimal morphology, taken by Holliday et al., is to increase the planarity and therefore crystallinity of rod-like A–D–A acceptors, which are otherwise too miscible with the polymer.[19,20] These examples highlight the importance of NFA molecular structure and conformation in OPV device performance, but also emphasize the difficulty in defining universal design rules for these different classes of molecules.

More broadly, the importance of molecular conformation in organic semiconductor properties is an increasingly important area of research. It has been shown that polymer backbone planarity can affect energy levels, BHJ morphology, energetic disorder, and charge transport. Attempts to control molecular conformation take two approaches, processing control or molecular structure design. Processing control involves controlling the active layer morphology, which in turn leads to molecular conformational rearrangement, e.g., increasing poly(3-hexylthiophene) (P3HT) crystallinity and backbone planarity in a BHJ via annealing.[21] Molecular structure design takes advantage of noncovalent intramolecular interactions that favor a certain conformation; for example, sulfur–fluorine interactions are known to increase conjugated backbone planarity of D–A copolymers, leading to higher crystallinity and charge carrier mobility.[22,23] The use of these so-called conformational locks may provide excellent control over organic semiconductor properties and allow for a more facile approach to controlling molecular conformation than attempting to remove rotatable single bonds between units.[24,25] More recently, these techniques have been applied to NFAs to control morphology and energetics. For instance, both Wu et al. and Liu et al. introduce alkoxy side chains to promote a more planar conjugated backbone, afforded by sulfur–oxygen interactions, leading to improved charge mobilities and device performance.[26,27] Tang and coworkers include hexyl side chains that hinder rotation about the D–A dihedral, leading to a favored conformation and weaker π–π stacking that in this instance improves compatibility with the donor polymer.[28] Although many molecular design rules have been applied to synthesize new NFAs to control their structure and conformation, the photostability of these new materials has not been properly studied.

In this work, we are concerned with the most successful class of NFAs, which are those based on linear A–D–A architectures such as IDTBR,[20,29] 3,9-bis(2-methylene-(3-(1,1-dicyanomethylene)-indanone))-5,5,11,11-tetrakis(4-hexylphenyl)-dithieno[2,3-d:2′,3′-d′]-s-indaceno[1,2-b:5,6-b′]dithiophene (ITIC),[30,31] and their derivatives.[32] IDTBR is composed of an electron-rich indacenodithiophene (IDT) unit with *n*-octyl side chains, flanked by the electron-withdrawing units: benzothiadiazole (BT) and 3-ethylrhodanine (**Figure 1**c). It has shown promising photostability and morphological stability and high performance with the semicrystalline homopolymer P3HT achieving a power conversion efficiency of 7%.[33] P3HT has often been used as a model system for studying organic solar cells,[34] and is still relevant for use in inexpensive large-scale modules due to it being readily available and having relatively lower cost compared to other higher-efficiency state-of-the-art donor–acceptor polymers. The best-performing P3HT/NFA device is realized when a third component, the acceptor IDFBR, is added in a ternary blend.[29] IDFBR is analogous to IDTBR but with an indenofluorene (IDF) core replacing IDT (Figure 1d).

Due to the different core units, the two acceptors adopt different molecular conformations as elucidated from single-crystal structure determination and density functional theory (DFT) simulations (Figure 1c,d) and reported in the literature.[20,29] IDTBR shows a planar backbone while IDFBR, due to steric clash between adjacent *ortho*-hydrogen atoms on the IDF and BT units, adopts a more twisted conformation with a dihedral angle of 33°. In this study, we investigate in detail how this minor change in chemical structure can cause significant changes in photostability, and then how this affects BHJ blend stability. For this, we employ P3HT as a model system to investigate the interaction of donor and acceptor and how this affects photostability in air. By elucidating the molecular origin of photostability, we provide guidance for the design of NFAs that avoid undesirable degradation pathways and create intrinsically stable photoactive BHJ layers that are resistant to the ingress of oxygen and moisture removing the need for encapsulation, which is often one of the more costly components of module fabrication.

In order to explore active layer degradation and stability, we utilize complementary spectroscopic techniques supported by quantum chemical simulations and structural probes. We also employ in situ Raman spectroscopy studies that enable us to track both vibrational and luminescence changes. This is important because in organic semiconductors, electronic excitations and molecular vibrations are strongly coupled due to distortion of the conjugated molecular backbone when in the excited or charged state. By measuring simultaneously the luminescence and vibrational transitions of the molecules, it is therefore possible to gain information about the conformation of molecules and the emission property of organic films.

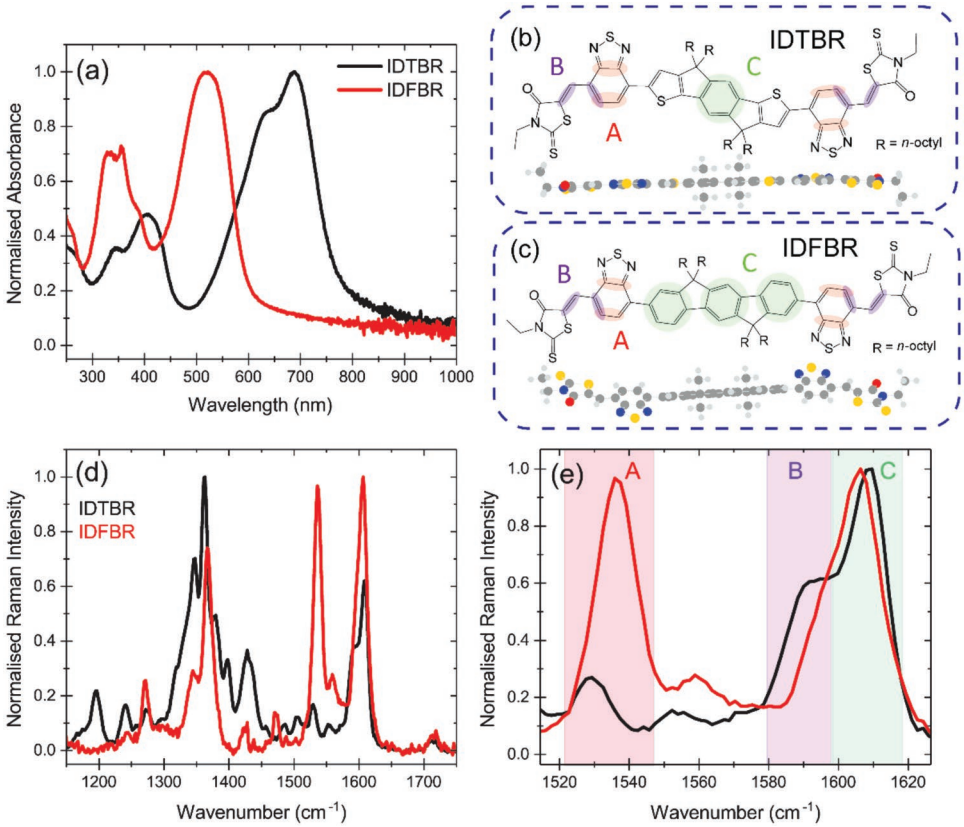

Figure 1. a) UV–vis absorption spectra of as-cast thin films of IDTBR and IDFBR chemical structures with vibrational mode assignment and DFT optimized structures of b) IDTBR and c) IDFBR. d) Normalized Raman spectra of as-cast films of IDTBR and IDFBR at 457 nm excitation; the highlighted region is the region shown in part (e). e) Normalized and assigned Raman spectra of IDTBR (black) and IDFBR (red dash) normalized to the phenyl mode, here labeled C.

In particular, under resonant excitation conditions (when the energy of the excitation photon matches the energy of a dipole-allowed electronic transition of the molecule), a strong enhancement in the Raman scattering intensity as well as photoluminescence (PL) occurs. Resonant Raman spectroscopy is highly sensitive to the molecular structure and conformation of π-conjugated molecules[35,36] and has been used previously to investigate the morphology[34] and stability of several bulk heterojunction OPV blends.[37–39]

We find that IDFBR is substantially less photostable than IDTBR in both nitrogen and air. By using in situ resonant Raman spectroscopy, we propose a three-phase degradation mechanism that explains this difference. The first step is a photoinduced conformational change, namely, an increase in the dihedral angle between the core and BT units. This leads to the second step of degradation, likely fragmentation or photo-oxidation, before reaching the third phase in which the chromophore is bleached completely. IDFBR, due to its more twisted backbone, is already prone to the second step of degradation, resulting in rapid photodegradation in both nitrogen and air.

Upon blending with P3HT, the two acceptors form different morphologies as observed previously. IDFBR is found to be more miscible with the polymer, while IDTBR forms a fairly well phase-separated morphology with P3HT. The photostability of the blend is also investigated, with both NFAs being stabilized by blending. On the other hand, P3HT degradation is accelerated by blending with twisted IDFBR, but when blended with planar IDTBR the polymer retains a similar stability to the neat films. The degradation of P3HT is found to go via a chemical oxidation that produces signatures that are similar to doping. This study highlights the importance of molecular design in NFA stability, and we propose that planarity and rigidity should be taken into account when designing stable acceptors. We also show how NFAs impact on the polymer stability in the photoactive layer blend, and suggest possible mechanisms for this.

2. Results and Discussion

2.1. Neat Film Morphology

To enable discussions on photostability and BHJ blends of the materials, we first discuss the neat film morphology and effect of annealing of NFAs.

Figure 1a shows the absorption spectra of as-cast IDTBR and IDFBR films. Both acceptors show two prominent absorption peaks within the visible range. Apparent absorption below the onset is due to scattering, induced by rough thin

films. The lower-energy peak, arising from the highest occupied molecular orbital (HOMO) → lowest unoccupied molecular orbital (LUMO) transition, is significantly redshifted for IDTBR, which is due to its more electron-rich core, raising the HOMO energy level, as well as a more planar molecular structure, as elucidated by DFT simulations (Figure 1b). This planar structure enables effective π-stacking in the solid state, resulting in a more crystalline morphology than IDFBR.[20,29] For both molecules, the HOMO is delocalized along the main conjugated backbone with most electron density sitting on the electron-rich core, while the LUMO is partially localized to the BT unit (Figure S1, Supporting Information). Due to the planarity of IDTBR, its HOMO and LUMO wavefunctions are more delocalized resulting in a large overlap between them, thereby enhancing oscillator strength of this transition. As opposed to IDTBR, the more twisted IDFBR (Figure 1c) has more localized HOMO and LUMO wavefunctions, resulting in stronger charge transfer (CT)-like character, as seen by the broad, less vibronic structure and a more typical symmetrical camel-back absorption associated with CT-like transitions in D–A organic molecules.[38]

Figure 1d shows the normalized Raman spectra of IDTBR and IDFBR at 457 nm excitation. There are common peaks between the two spectra: a carbonyl peak at ≈1710 cm^{-1} arises from the rhodanine groups, the peak at ≈1600 cm^{-1} is assigned to the fused phenyl groups in the core of both molecules, and BT peaks are found at ≈1530 and ≈1350 cm^{-1}. The phenyl peak of IDFBR has a much larger relative intensity due to there being three phenyl rings in the IDF core, compared to just one in IDTBR. There are also clear differences between the spectra arising from the thiophene peaks present (1380–1450 cm^{-1}) for IDTBR, which are not observed for IDFBR. A full spectral assignment of these spectra is given in Figure S2 in the Supporting Information. Figure 1e shows the assignment of three key peaks, with the corresponding bonds highlighted in Figure 1b,c. Peak A, centered at 1529 cm^{-1} for IDTBR, is localized to the BT unit of the acceptor and is assigned to the symmetric stretch of the C—C bonds within the benzene ring. Peak B, at 1592 cm^{-1}, is assigned to the alkene bond between the BT and rhodanine units, and peak C, at 1609 cm^{-1}, is a vibration localized to the phenyl rings within the core IDT unit. IDFBR has equivalent A and C peaks at 1536 and 1606 cm^{-1}, respectively, with peak B appearing as a low-frequency shoulder of peak C at 1595 cm^{-1}. Peak assignment has been guided by DFT simulations, and comparison with the literature.[40,41] For a full description of the morphology changes upon annealing of these films, please see Figure S3 in the Supporting Information.

2.2. Neat Film Photostability

The absorption spectra of fresh and degraded as-cast neat films of the two acceptors are shown in **Figure 2**a,b. Degradation has been carried out using a solar simulator at 1 sun illumination within a temperature-controlled environment in air. After 8 h of illumination, there is a bleaching and slight blueshift of the lower-energy peak of IDTBR. Similarly, the low-energy transition of IDFBR shows the same bleaching and blueshift but this is apparent after just 1 h of illumination. After an equivalent 8 h of illumination, there is a near-complete bleaching of absorption within the visible range, indicating that the more amorphous, twisted IDFBR is much less photostable in air than the planar, crystalline IDTBR.

The normalized Raman spectra of fresh and degraded acceptors are shown in Figure 2c,d. After 8 h of illumination, IDTBR shows an increase in relative intensity of peaks A and B with respect to peak C. To investigate the origin of these spectral changes, Raman spectra of IDTBR at different IDT–BT torsion angles were simulated. It was found that increasing the IDT–BT dihedral angle resulted in spectral changes consistent with those observed experimentally. Similarly, IDFBR also shows changes in the relative peak intensity of peak A upon degradation, but the opposite change is observed. This opposite change is observed in both the experimental and calculated spectra, but the reasons for this are not clear. We suggest this may be due to the nature of the phenyl peak to which we normalize. IDFBR has three core phenyls contributing to this peak, while IDTBR has one phenyl ring flanked by thiophene units. Therefore, the change in electron density upon conformational change may not be the same in both cases, leading to the different variations in relative Raman intensities. Another possibility is that the BT unit is affected differently during conformational change due to the noncovalent interactions between the BT unit and the neighboring thiophene in the IDTBR core; this could again alter the change in electron density upon conformational change, leading to the different peak changes. After 1 h of illumination, IDFBR already shows a 41% decrease in the relative intensity of peak A, with respect to peak C, which itself shifts 2 cm^{-1} to higher frequencies. DFT calculations confirm that these peak changes are again consistent with a higher torsion between the IDF and BT units inducing a more twisted structure. These observations suggest that illumination of both of these NFAs in air induces the same molecular conformational change, namely, a rotation about the core–BT dihedral. Such changes in BT relative peak intensity (peak A) and phenyl peak shift (peak C) have previously been correlated to a decrease in backbone planarity for the polymer F8BT by Schmidtke et al.[40] Interestingly, this molecular-scale conformational change does not affect the macroscopic surface morphology of IDTBR (see atomic force microscopy (AFM) images in Figure S4 in the Supporting Information).

The bleaching of absorption observed in the lower-energy transition for the as-cast films can be understood by this molecular conformational change. The CT-like character of this low-energy transition has been described by Jespersen et al. for conjugated polymers containing BT units.[42] IDFBR with its more twisted molecular structure has more of this CT-like behavior, with the HOMO and LUMO being more spatially confined to the donor and acceptor units, respectively. In contrast, the HOMO and LUMO of IDTBR, due to its planar structure, are more delocalized along the entire molecule, but still retain some CT character. This more delocalized transition has a higher oscillator strength, due to increased orbital overlap (**Figure 3**c,d). It is consistent with the study by Vezie et al., who show that a longer polymer persistence length, which is correlated to planarity, is needed for a higher optical density.[43] If upon continuous light illumination and

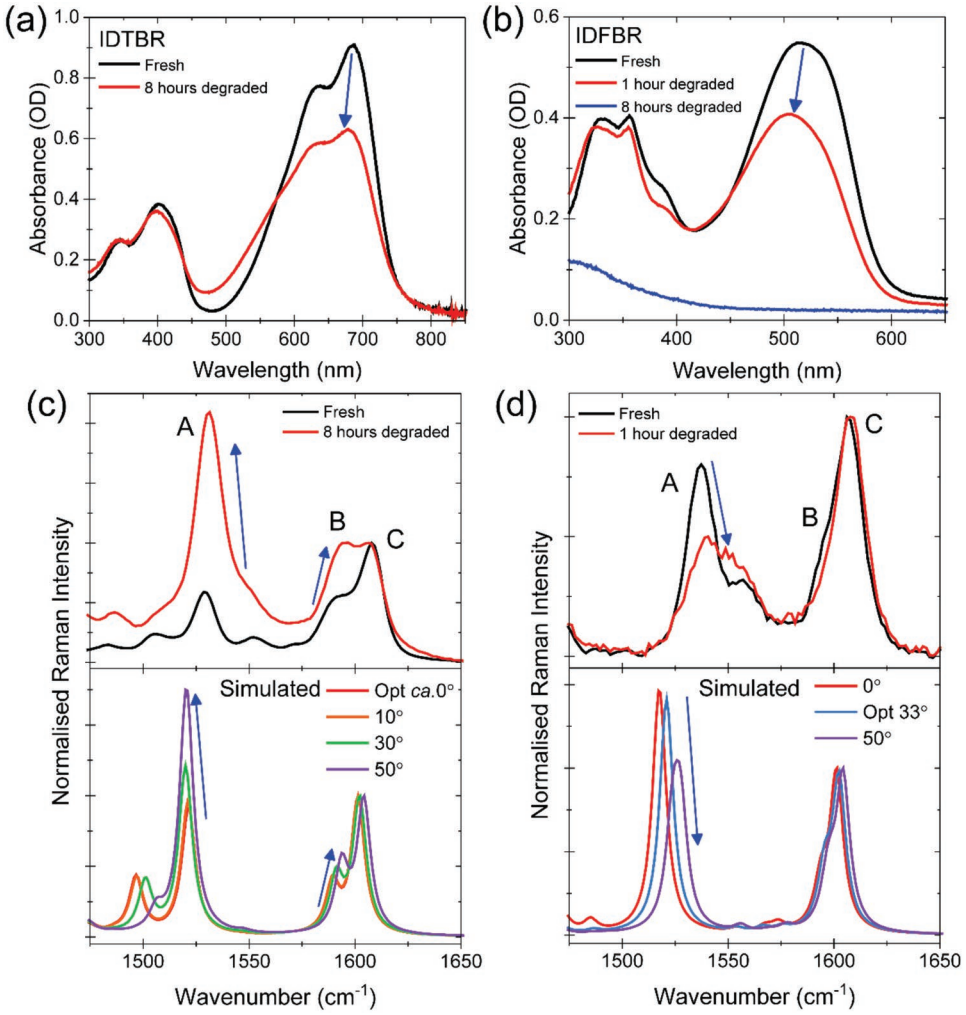

Figure 2. Absorption spectra of fresh and degraded as-cast films of a) IDTBR and b) IDFBR. Top: normalized Raman spectra of c) IDTBR at 488 nm excitation and d) IDFBR at 457 nm excitation of fresh and degraded as-cast films, with vibrational peak assignment consistent with Figure 1; bottom: normalized DFT simulated Raman spectra of c) IDTBR and d) IDFBR at various core–BT dihedral angles. The chemical structures show the dihedral angle in question. The optimized angle for IDTBR is ≈0° while that for IDFBR is ≈33°.

degradation there is a twisting about the donor–acceptor dihedral angle, it will cause more localization of the HOMO and LUMO wavefunctions to the donor and acceptor units, respectively, reducing the transition oscillator strength and thus quenching the lowest-energy absorption transition, as observed. The observed blueshift of both IDTBR and IDFBR is due to the decreased effective conjugation length of the twisted molecules. Simulated UV–vis spectra for the planar and twisted nonfullerene acceptors support this hypothesis, showing that the lower-energy transition is bleached and blueshifted upon increasing the core–BT torsion angle (Figure S5, Supporting Information).

We note that the higher-energy peak remains relatively unchanged during degradation, while the lower-energy CT-like absorption that involves the BT unit is selectively quenched in both molecules. This selective degradation of the lower-energy absorption can be related to much stronger absorption of low-energy photons (<450 nm) in both molecules (Figure S6, Supporting Information), but also more importantly to its CT-like character involving the BT unit, which we have shown is responsible for degradation. Interestingly, the more significant bleaching of the lower-energy absorption transition is observed in IDFBR, which may originate from the higher-energy photons (450–600 nm) involved in this transition than IDTBR (500–750 nm), as reported for blue organic light-emitting diodes.[44,45]

To further investigate the chemical processes undertaken by these materials under illumination in air, mass spectroscopy was conducted to probe for degradation products. After 1 h of degradation, IDFBR shows clear molecular fragmentation that becomes more pronounced after 8 h of degradation (Figure S7, Supporting Information). This is consistent with the near-complete bleaching of absorption seen for the 8 h degraded IDFBR film. The PL spectrum of fresh IDFBR shows an emission at 650 nm, while the 8 h degraded film shows only a blueshifted emission at 550 nm (Figure S8, Supporting Information), which we assign to emission from

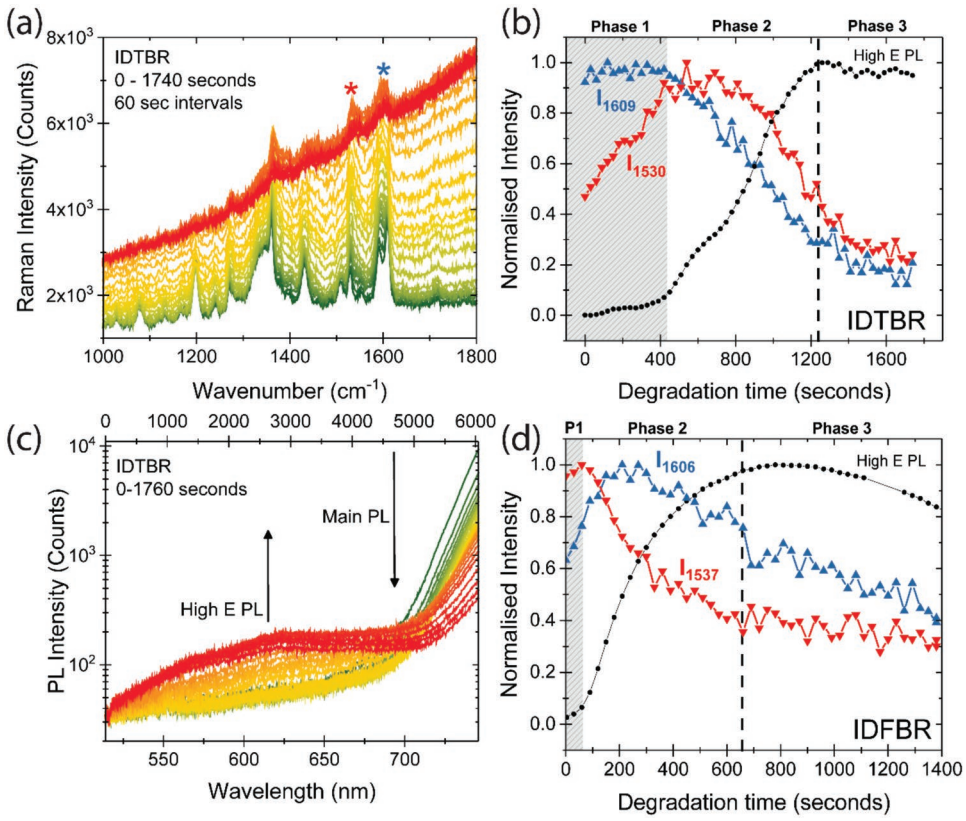

Figure 3. a) Raw in situ Raman spectra at 457 nm excitation of a neat, annealed IDTBR film shown as a function of laser illumination time starting with green spectra and progressing to red; the red and blue stars indicate the positions of the vibrational modes labeled A and C in Figure 1. b) Normalized data extracted from part (a) including intensities of peaks A and C (red and blue lines) and the increase in background PL (filled black circles). c) In situ PL spectra of the same IDTBR film taken at 514 nm excitation as a function of laser illumination time. d) Extracted information from in situ Raman spectra of a neat IDFBR film using 457 nm laser probe taken at increasing laser illumination time. It should be noted that plots (b) and (d) show the absolute peak intensities after PL background removal; these values are then normalized to allow for concurrent plotting.

the observed fragmentation products that are assumed to have a reduced effective conjugation length and therefore higher optical band gap. Fragmentation is clearly occurring within the IDFBR film, alongside the conformational change suggested above.

The mass spectrum of IDTBR after 8 h of illumination in air (Figure S7, Supporting Information) shows significantly less fragmentation but interestingly there are small peaks appearing at 1340 and 1356 m/z, which are 16 and 32 m/z units above the molecular ion peak at 1324, indicating the addition of oxygen to the structure, suggesting chemical oxidation has occurred. Due to the small signatures of oxidation and fragmentation in degraded IDTBR, it is concluded that although these processes are occurring, they are minor processes that cannot account for the large Raman changes observed upon degradation.

So far, the discussion has been concerned with as-cast films. As described in the supporting discussion (Figure S3, Supporting Information), for IDFBR, thermal annealing is shown to make no difference to the molecular conformation or morphology, and its photostability is not significantly affected. On the other hand, IDTBR is shown to increase in crystallinity upon thermal annealing, which stabilizes the film toward photodegradation in air (Figure S9, Supporting Information). This is observed as a reduction in the bleaching of absorption after the same degradation time as the as-cast films. Raman spectra of the annealed IDTBR show the same changes seen in the as-cast films, but they are less pronounced, indicating that the same degradation mechanism is occurring, albeit at a slower rate.

2.3. In Situ Degradation

In situ degradation using the laser excitation as an accelerated degradation source was carried out to further investigate the photodegradation processes of these acceptors. Using the Raman experimental setup, it is possible to track Raman peaks and PL as a function of laser illumination time. The degradation laser used is monochromatic and has an approximate power density three orders of magnitude larger than 1 sun illumination allowing for accelerated degradation studies.

Figure 3a shows the raw Raman spectra obtained during accelerated (see the Experimental Section) in situ degradation of annealed IDTBR. With increasing illumination time, there is a delayed increase in the background (caused by increasing PL), a change in the relative peak intensities, and toward longer times a reduction in Raman peak intensity of all peaks. For a more in-depth analysis of these spectra, the peak intensities

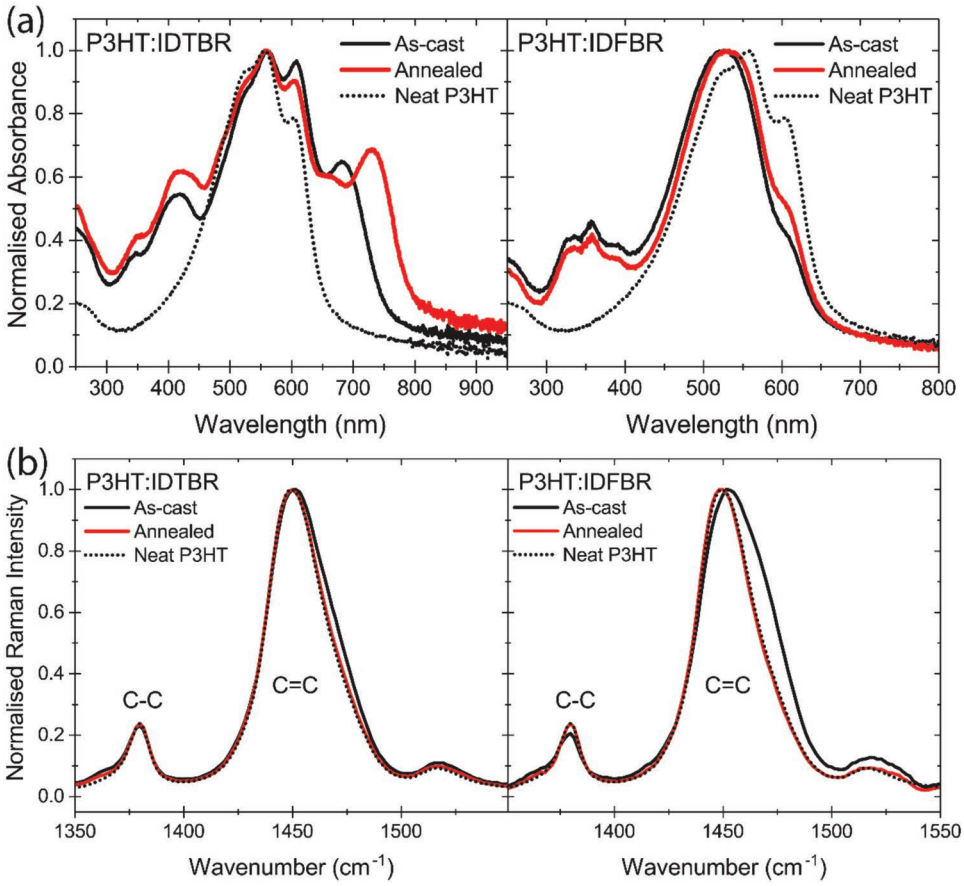

Figure 4. a) Normalized UV–vis absorption spectra of as-cast and annealed (130 °C, 10 min) P3HT:IDTBR (left) and P3HT:IDFBR (right) 1:1 blend films plotted with neat annealed P3HT absorption for reference. b) Normalized Raman spectra of P3HT:IDTBR (left) and P3HT:IDFBR (right) as-cast and annealed blend films at 457 nm excitation. The P3HT:IDFBR spectra have been deconvoluted to show only the vibrational modes of P3HT; again neat, annealed P3HT is plotted for comparison.

of the BT and phenyl peaks (starred) and the PL background are extracted and summarized in Figure 3b. We observe three distinct phases in the degradation process. Phase 1 (0–400 s) is predominantly characterized by the molecular conformational change, namely, the rotation about the IDT–BT dihedral, as observed in the solar simulator degraded samples. The Raman intensity of the BT peak (A) at 1530 cm^{-1} increases to a maximum, while the intensity of the phenyl peak (C) at 1609 cm^{-1} and PL background remain constant, indicating no loss of the chromophore. **Figure 4**c shows that the main emission from the $S_1 \rightarrow S_0$ transition (>700 nm) is quickly quenched during this first phase of degradation, which is consistent with the PL quenching observed in the solar simulator degraded samples (Figure S8, Supporting Information). Phase 2 (400–1200 s) is defined as the point at which the background PL in Figure 4a begins to increase, while the Raman intensity of the 1609 and 1530 cm^{-1} peaks begins to be quenched. This increase in background PL is due to the appearance of a new distinct high-energy PL peak at ≈625 nm, which is orders of magnitude weaker than the initial $S_1 \rightarrow S_0$ emission. This quenching of the IDTBR vibrational modes and appearance of the new high-energy PL peak suggest a strong change to the chromophore of the molecule upon continuous illumination. Phase 3 (>1200 s) begins when the high-energy PL has reached a maximum with no more degradation product forming after this point. The Raman peak intensities of the initial molecule are now negligible, indicating that the IDTBR molecules are heavily degraded, and the initial chromophore has been almost completely bleached. If degradation were continued (not shown here), this product PL begins to decrease, relating to breakdown of the degradation product. Phase 3 shows an extreme of degradation and devices containing IDTBR would have degraded long before this stage of molecular degradation.

Similar Raman and PL spectra from in situ degradation studies of IDFBR are shown in Figure S9 in the Supporting Information. Interestingly, it also shows a similar three-phase degradation process (Figure 2b), although the first phase is dramatically accelerated, and phases 1 and 2 overlap. Phase 1 again consists of a quenching of the main $S_1 \rightarrow S_0$ emission, and a rotation about the IDF–BT dihedral as seen by the relative intensity of the phenyl and BT peaks. The background PL begins to increase with the first few measurements. By following the whole PL spectrum as a function of degradation time, there is also a slight blueshift of the main PL peak, which could be caused by the increasing band gap expected for more twisted molecules. However, in the 8 h solar degraded

sample, there is a distinct high-energy emission at 550 nm (Figure S8, Supporting Information), even after the IDFBR absorption is quenched, suggesting that this is a new emissive species formed upon degradation. This is confirmed by PL decay measurements of the two samples, which show different PL decay lifetimes for the fresh and degraded samples with the fresh sample dominated by a monoexponential process while the degraded decay requires multiple exponential components to fit (Figure S11, Supporting Information). Similarly to IDTBR, this high-energy PL can be assigned to a degradation (fragmentation)-induced product, with a reduced conjugation length. Phase 3 is more distinct for IDFBR, being defined at the peak of high-energy PL, after which this PL begins to decrease.

The origin of the conformational change observed is unlikely to be purely photoinduced, as simulated excited states of IDTBR and IDFBR in gas phase show planar geometries (Figure S12, Supporting Information). However, noncovalent interactions between environmental and conjugated molecules have previously been shown to affect the potential energy surface (PES) of conjugated polymers.[46] A disruption of the smooth PES allows for many more possible conformations to be adopted. We therefore propose that the conformational change observed here for IDTBR and IDFBR is caused by a similar interaction with environmental species, most likely oxygen. This change in dielectric surroundings then allows for new minimum energy structures to be adopted. We show that light is required for this conformational change to occur, and therefore suggest that this noncovalent interaction is between excited or charged species of the conjugated or environmental molecules, which are formed upon photoexcitation. Nikolka et al. show that for the polymer IDTBT, a more twisted backbone conformation is possible in the presence of these environmental species.[46] This allowed increase in the IDT–BT dihedral angle is analogous to the conformational change observed here for IDTBR. This may indicate that this is a common phenomenon for conjugated systems containing BT units. This is supported by our initial photodegradation studies on IDTBT, which indicate that a similar conformational change, i.e., IDT–BT torsion, may occur upon degradation of the polymer (Figure S13, Supporting Information). Based on microsecond transient absorption measurements, we also propose that once the molecular conformation change occurs, allowing interactions with oxygen, the dominant mechanism of degradation of these NFAs is triplet-mediated formation of reactive singlet oxygen (see Figure S14 in the Supporting Information for details).

Interestingly, if we degrade IDTBR in an inert N_2 environment, it is found to be stable toward this degradation mechanism (Figure S15, Supporting Information), signifying the importance of oxygen in the conformational change–initiated degradation process. It should also be noted that this degradation mechanism also occurs in EH-IDTBR, an isomer of O-IDTBR with branched ethylhexyl side chains, as shown in Figure S13 in the Supporting Information. Unlike IDTBR, IDFBR degrades quickly under illumination in an inert atmosphere, showing similar Raman changes to those observed in air (Figure S16, Supporting Information). The spectral changes observed are thus due to fragmentation signatures, as indicated previously in the mass spectra of the degraded samples in air. As IDFBR is already twisted, it is already prone to the second step of rapid photodegradation.

The results obtained so far help us to understand the improvement of stability of IDTBR upon increasing molecular planarity and crystallinity. The conformational change and diffusion of oxygen will both be restricted by a more closely packed molecular lattice, explaining why the annealed IDTBR films show an improvement in stability. This improvement of stability with increasing crystallinity has also been observed for the small molecule donor benzodithiophene terthiophene rhodanine (BTR), which similarly involves a conformational change upon degradation in nitrogen.[39] Therefore, our observation reinforces the importance of crystallinity of NFAs for OPV stability.

2.4. Blends with P3HT

Having investigated the degradation mechanism of IDTBR and IDFBR in neat films, we now turn our attention to their morphology and stability when blended with P3HT.

Absorption spectra of the as-cast and annealed blends are shown in Figure 4a, with annealed neat P3HT absorption shown for comparison. Neat P3HT itself shows no noticeable change in absorption upon annealing at 130 °C for 10 min (Figure S17, Supporting Information). However, in the P3HT:IDTBR blend, there is a clear increase in IDTBR crystallinity upon annealing, as shown by a 47 nm redshift of the IDTBR peak at 682 nm, analogous to the shift observed in the neat film. By deconvoluting the as-cast P3HT:IDTBR blend spectra, we observe a decrease in the relative intensity of the shoulder at 600 nm (assigned to P3HT aggregation[35]) compared to the neat P3HT films, which indicates that P3HT aggregation is being somewhat inhibited by blending with IDTBR. Upon annealing the P3HT:IDTBR blend, there is an increase in the relative intensity of this shoulder showing an increase in P3HT aggregation. This is more easily discerned in the P3HT:IDFBR blend, in which a shoulder at 600 nm shows a significant increase in relative intensity upon annealing, again signifying an increase in P3HT aggregation. IDFBR absorption shows no change upon annealing in the blend analogous to the neat IDFBR films.

Figure 4b comprises the normalized Raman spectra of P3HT within the blends. To investigate the P3HT peaks, the P3HT:IDFBR spectra were deconvoluted while this was unnecessary for the IDTBR blend due to the relatively small Raman cross section of IDTBR compared to P3HT. Tsoi et al. show that as P3HT order (i.e., backbone planarity) is reduced, there is a shift of the main C=C Raman peak (≈1450 cm^{-1}) to higher frequencies, and the relative intensity of the C−C peak (≈1380 cm^{-1}) decreases as the effective conjugation length and therefore π-electron delocalization is reduced.[35] A very small increase in the full width at half maximum (FWHM) (1 cm^{-1}) of the P3HT C=C mode is observed in the as-cast P3HT:IDTBR blend compared to neat as-cast P3HT, suggesting there is only a very minor disruption of P3HT molecular order by blending with planar IDTBR. In contrast, the P3HT C=C peak in the as-cast P3HT:IDFBR blend shows much larger broadening (5 cm^{-1}) and a 4 cm^{-1} peak shift to higher frequencies, indicating a significant disruption of P3HT order; i.e., twisted IDFBR is more miscible

with P3HT. Upon annealing, P3HT order in both the P3HT and P3HT:IDTBR (Figure 4b) films increases slightly, shown by a reduction in the main P3HT peak FWHM of 3 cm^{-1}. Annealing the P3HT:IDFBR blend results in a shift of the C=C peak to lower frequencies and a significant narrowing of the FWHM signifying a restoration of P3HT order upon annealing (Figure 4b). These findings are supported by the PL spectra of the as-cast and annealed polymer, and blend films that are shown in Figure S18 in the Supporting Information. The P3HT and IDTBR components of PL in the blend follow their neat film PL changes upon annealing indicating a well-separated morphology. In the P3HT:IDFBR blend, however, there is substantial increase in intensity of the overlapping emission feature, which is indicative of phase separation.[34] AFM images (Figure S18, Supporting Information) of both blends show an increase in roughness upon annealing confirming increased P3HT and IDTBR crystallinity.

Morphological studies carried out previously using differential scanning calorimetry and X-ray techniques also show that IDFBR is more miscible with P3HT than IDTBR.[20,29] Our observations confirm the idea that the twisted IDFBR molecules are miscible with P3HT, leading to a disruption of polymer molecular order. Upon annealing there seems to be a certain degree of phase separation between IDFBR and P3HT resulting in, to some degree, the recovery of P3HT molecular order and aggregation. The planar IDTBR molecules, on the other hand, are less miscible with P3HT, so no significant disruption of P3HT molecular order in the blend is observed in the absorption, Raman, or PL spectra. P3HT and IDTBR retain their neat film properties in the as-cast blend films and exhibit the same annealing effects indicating that P3HT and IDTBR form a well phase-separated morphology in blend, even before thermal treatment. This highlights the importance of acceptor molecular structure in blend morphology.

2.5. Blend Stability

To investigate the photostability of the blends, annealed blend and neat P3HT films were degraded under 1 sun illumination in air, in the same way as the neat NFA films. **Figure 5**a shows the absorption spectra of P3HT:IDTBR blend films before and after degradation. There is a 27% intensity bleaching of the P3HT absorption centered at ≈550 nm, analogous to the 25% bleaching of intensity upon equivalent degradation of neat P3HT (Figure S19, Supporting Information). However, the IDTBR absorption is not bleached upon degradation in the blend after 8 h. Above, we observed that annealing the neat IDTBR film led to an increase in stability and there is only minor absorption bleaching after 8 h of degradation (Figure S9, Supporting Information). The lack of bleaching in the blend film after equivalent degradation suggests that this stability of the annealed neat film is maintained or slightly improved in the blend, indicating that the well-separated morphology of P3HT and IDTBR leads to the neat film properties being preserved in the blend.

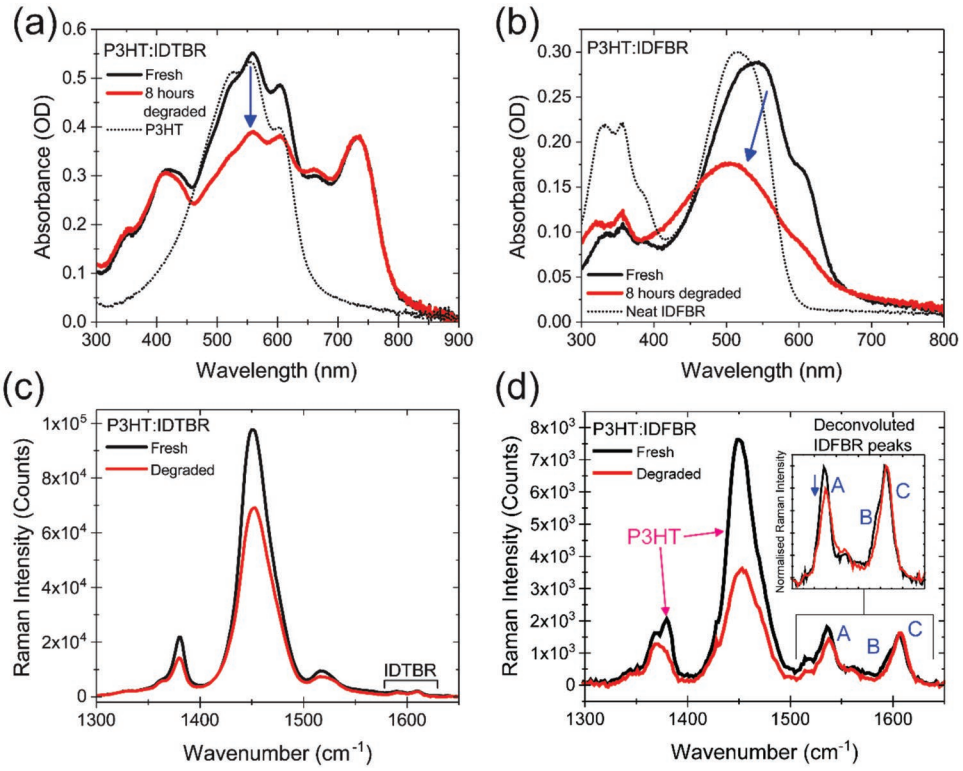

Figure 5. UV–vis absorption spectra of fresh and degraded (solar illumination in air) a) P3HT:IDTBR and b) P3HT:IDFBR blend films with fresh P3HT (a) and fresh IDFBR (b) absorption spectra for reference. c) Baseline corrected Raman spectra of P3HT:IDTBR at 457 nm excitation. d) Baseline corrected Raman spectra of P3HT:IDFBR at 457 nm excitation; the main P3HT modes are labeled, while the inset shows the normalized and deconvoluted IDFBR Raman peaks within the blend, labeled A, B, and C.

Figure 5b shows the absorption spectra of P3HT:IDFBR before and after solar illumination in air. There is a strong bleaching and blueshift of the main overlapping absorption band, while the IDFBR absorption peak between 300 and 400 nm is not bleached. It is important to notice that after 8 h of degradation of neat IDFBR there was a complete bleaching of both absorption bands of IDFBR (Figure 2a), whereas in the blend there is still clear high-energy IDFBR absorption, indicating that IDFBR is stabilized in the blend. In contrast, the intensity of the P3HT aggregate shoulder at 608 nm is significantly reduced by 50% in the blend whereas in the neat film this is bleached by only 30%, suggesting P3HT becomes less stable, with its degradation accelerated when blended with IDFBR. P3HT absorption quenching of this nature has been observed and is attributed to a reduction in π-conjugation length caused by radical oxygen–driven oxidation of the thiophene moieties.[47–49] Akin to the absorption changes, the Raman spectra of the fresh and degraded samples in Figure 5c,d show a selective bleaching of the P3HT modes (≈1380, 1450, and 1515 cm^{-1}). The intensity of the main P3HT peak is quenched significantly more when blended with IDFBR (>50%) compared to when blended with IDTBR (≈30%), reinforcing the claim that the twisted acceptor reduces the polymer stability.

Now, we look at the changes in the acceptors. The deconvoluted Raman spectra of IDFBR in the blend are shown in the inset of Figure 5d. After 8 h of degradation, there is a decrease in the relative intensity of the BT peak (A) at 1536 cm^{-1}, and a narrowing and slight shift of peak C to higher frequencies, indicating the same degradation process as observed in the neat film. Although these changes are much smaller than those in the neat IDFBR film (Figure 2d), the result confirms the same conformational change occurring during photodegradation in the blend and much less stable nature of the twisted IDFBR acceptor. Similarly to the neat IDTBR films, both blends show no significant change to the surface morphology upon degradation (Figure S4, Supporting Information).

The observations so far allow us to conclude that IDFBR is stabilized in the blend; to investigate whether this is also true for IDTBR, accelerated in situ degradation studies on the P3HT:IDTBR blend were carried out. **Figure 6**a shows the Raman spectra obtained during in situ degradation of the blend using 633 nm illumination. At this wavelength, both P3HT and IDTBR have significant absorption. There is an instant bleaching of the P3HT C=C peak, with a slight broadening to lower frequencies (Figure S20, Supporting Information). The intensity of peak C of IDTBR (1608 cm^{-1}) initially stays constant while the relative intensity of peak A (1530 cm^{-1}) increases in intensity, analogous to the initial Raman peak changes observed during in situ neat film degradation and attributed to a molecular conformational twisting of the IDTBR backbone (Figure 3a,b). The inset shows that this initial molecular conformational change is followed by a quenching of all IDTBR peaks, signifying that the three-phase degradation process observed in the neat films is also occurring in the blend.

It is important to consider the impact of such conformational changes of the NFA molecules on the photostability of photovoltaic blends. Interfacial energetics, determined by donor and acceptor energy levels (in particular, the LUMO level of the acceptor), are critical for photophysical processes of photovoltaic devices such as charge generation. The conformational changes of NFAs toward more twisted structures upon illumination in air would shift their LUMO energy levels to shallower energies (Figure S4, Supporting Information), reducing the interfacial energy offset between donor and acceptor affecting photophysical processes and their stability. In ongoing work, we demonstrate that the donor polymer stability in the blend is dependent on the LUMO level of the acceptors, which explains why P3HT is less stable when blended with the acceptor with the shallower LUMO, here IDFBR.

Accelerated degradation studies using the 457 nm excitation as a degradation source were also carried out (Figure 6b), for comparison with the neat film in situ degradation outlined in Figure 3. As with 633 nm degradation, there is a significant bleaching of the P3HT C=C mode. Surprisingly, after ≈30 min of 457 nm illumination, there are negligible changes in the IDTBR Raman peaks, in contrast to the neat films that show clear conformational changes within 30 s of 457 nm illumination. P3HT absorbs strongly at 457 nm while IDTBR has only a small absorption, so one would expect a disproportionate degradation of P3HT; however, it is shown that at this wavelength rapid degradation of IDTBR is also possible in the neat film. We therefore suggest that IDTBR is more stable in the blend compared to the neat film. Our results indicate that both NFAs are stabilized in the blend, and we assign this stabilization to

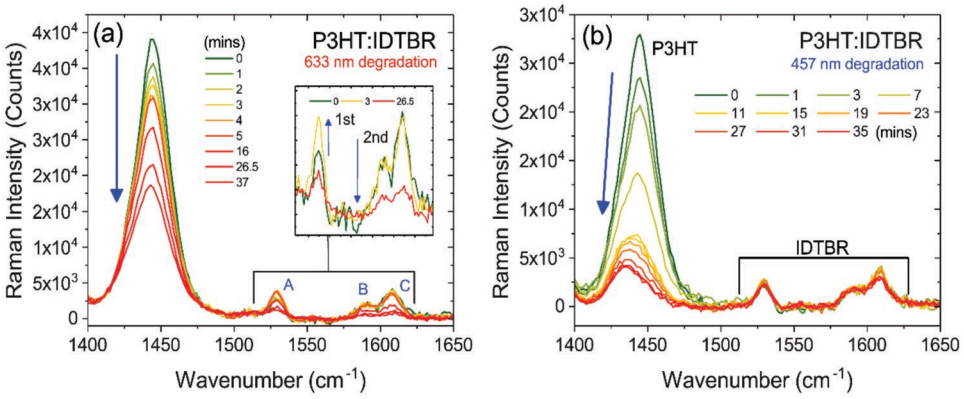

Figure 6. Baseline corrected in situ Raman spectra at increasing laser illumination times in air. At time 0, the films have already been illuminated for 8 h in a solar simulator in air; the probe excitation for both measurements is 633 nm. The degradation lasers were a) 633 nm and b) 457 nm.

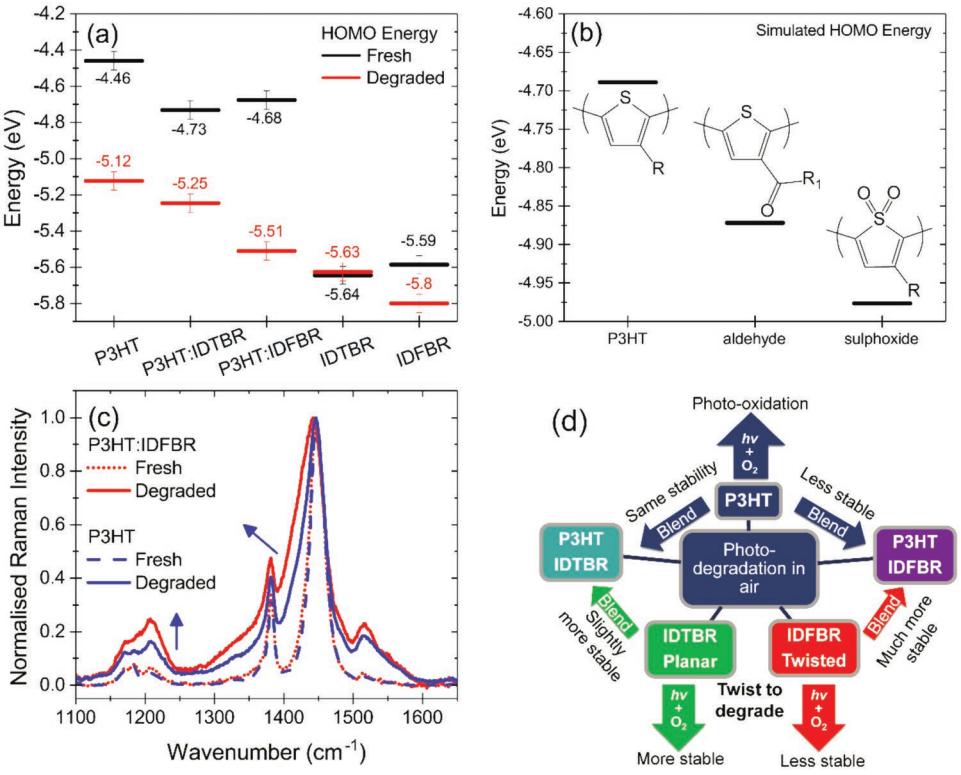

Figure 7. a) HOMO energy levels obtained using APS of fresh and degraded films on ITO. b) Simulated HOMO levels (DFT, B3LYP, 6-31G(d,p)) of P3HT pentamers with different potential oxidation products on the central monomer as shown in the inset chemical structures. c) Normalized Raman spectra of neat P3HT and P3HT:IDFBR at 785 nm excitation. d) Summary of stabilization and destabilization processes in the blends.

excited-state quenching via charge generation with the polymer, reducing the excited-state degradation observed in the neat films.

To investigate P3HT photodegradation further, HOMO energy levels were measured using air photoemission spectroscopy (APS). **Figure 7**a shows the extracted HOMO energy levels for fresh and degraded films (APS spectra can be found in Figure S21 in the Supporting Information). There is a deepening of the P3HT HOMO level from 4.50 ± 0.05 to 4.70 ± 0.05 eV upon blending with the NFAs. This may be due to the NFAs disrupting P3HT crystallinity as observed by the reduced aggregate shoulder in the deconvoluted absorption spectra, and similar to previous reports of P3HT energy levels as a function of crystallization.[50] The measured HOMO energy levels of the as-cast films of both IDTBR and IDFBR are ≈5.60 eV. Upon degradation, there is a further deepening of the P3HT HOMO level and additionally a reduction in photoemission yield. Deepening of the HOMO level by 0.65, 0.50, and 0.85 eV is measured for P3HT, P3HT:IDTBR, and P3HT:IDFBR films, respectively. The most dramatic change is observed for the P3HT:IDFBR blend, again indicating that P3HT degrades faster in the presence of IDFBR. By blending P3HT with IDTBR, the stability of P3HT is slightly improved relative to the neat film. To see whether these changes are caused by photo-oxidation, as suggested above, the HOMO energy level of P3HT and some potential oxidation products[47,48] were simulated. Both oxidized species show a deeper HOMO level than P3HT (Figure 7b), highlighting the electron-withdrawing effect of the electronegative oxygen atom on electron density. They also show smaller optical band gaps than P3HT (Figure S22, Supporting Information).

The nature of photodegradation of P3HT was further investigated by resonant Raman spectroscopy using 785 nm excitation, which will be resonant with the oxidized species with a smaller optical band gap (Figure 7c). After 8 h of degradation of the neat and blend films, the main P3HT C=C peak broadens to lower frequencies and there is an increase in relative intensity of the C−C peak at ≈1200 cm^{-1}. In the P3HT:IDFBR blend, the broadening of the C=C peak and growth of the peak at 1200 cm^{-1} occur to a much greater extent, indicating faster degradation of P3HT in the IDFBR blend, confirming our claim that P3HT becomes much less stable when blended with twisted IDFBR. The Raman simulations of the P3HT pentamer containing a sulfoxide unit show similarities to those of the experimentally degraded P3HT (Figure S22, Supporting Information), thus providing a possible origin to these observations; these spectral changes have been previously observed upon P3HT degradation in air.[51,52] Note that the Raman features and deeper HOMO appearing in photo-oxidized samples also have a close resemblance with polaronic species formed upon chemical doping of P3HT.[53–55] Figure 7d summarizes the stabilization and destabilization effects of IDTBR, IDFBR, and P3HT observed between their neat and blend films.

In Figure S23 in the Supporting Information, we show the normalized device characteristics for OPV devices fabricated with P3HT:IDTBR and P3HT:IDFBR active layers with the same protocol previously reported.[29] The IDFBR devices show a much

faster degradation than those containing IDTBR, highlighting the importance of using a stable active layer blend in devices.

3. Conclusions

In this work, we have investigated the effect of molecular structure on the photostability of two nonfullerene acceptors, IDTBR and IDFBR. We have found that under illumination in air these molecules undergo a three-phase degradation process. Initially, a photoinduced conformational change occurs, driven by noncovalent interactions with environmental molecules. This allows for a second step of degradation, either photo-oxidation or fragmentation, disrupting the molecular chromophore. This is then followed by the third phase in which the initial chromophores of the molecules are completely bleached. These findings suggest that planarity of the conjugated backbone and crystallinity of these small molecule acceptors are beneficial to neat film photostability in both ambient and inert environments. Furthermore, the molecular conformation is found to be important for understanding the miscibility of IDTBR and IDFBR with the semicrystalline donor polymer P3HT and the photostability of their blends. The amorphous, nonplanar IDFBR is more miscible than planar IDTBR with P3HT. When blended, much faster and significant photodegradation of P3HT is observed in P3HT:IDFBR blend compared to P3HT:IDTBR blend. The same three-phase degradation process of NFAs is also found in the blends although both show their degradation is slowed down. These results highlight the important role of NFA's molecular structure in photostability of photovoltaic blends.

Based on our observations, we propose molecular design considerations for A–D–A nonfullerene acceptors: first, a planar structure of the conjugated backbone is important for stability and not just for optimizing morphology for efficiency; second, we speculate that if this planarity was frozen, by the use of fused systems, or by intramolecular interactions, i.e., the so-called conformational locks discussed above, it would be possible to inhibit the degradation mechanism observed. With interest in utilizing these conformational locks increasing, it is important to investigate their role in stability. We have also introduced some results from molecules containing BT groups that may show similar degradation pathways. We therefore raise the question as to whether there is an intrinsic stability problem when using BT units within conjugated molecules, although further studies are required.

4. Experimental Section

Sample Preparation: The syntheses of IDTBR and IDFBR have previously been reported.[29] Two batches of regioregular P3HT were used within the blends although both were of a similar molecular weight (MW) and regioregularity (MW = 51 kDa, ≥96% regioregularity and MW = 36 kDa, >99% regioregularity). It has recently been shown that P3HT:IDTBR devices have a P3HT MW–dependent performance due to the sensitivity of morphology to molecular weight.[33] From the measurements, very slight differences in morphology depending on sample batch studied but without any major influence on the conclusions presented in this work were observed. Neat NFA solutions were prepared at a concentration of 12 mg mL^{-1} in chloroform, while neat P3HT and 1:1 P3HT:NFA blends were dissolved in chlorobenzene at 10 and 20 mg mL^{-1}, respectively. All solutions were stirred overnight at 60 °C before thin films were spin coated onto clean glass, indium tin oxide (ITO), or fused quartz substrates to give films with a thickness of 50–100 nm measured with a Dektak profilometer. Films were annealed within a N_2 atmosphere at 130 °C for 10 min. Degradation of the samples was carried out using a Solaronix solar simulator (Class AAA), at 1 sun illumination (AM1.5) in air with a temperature maintained at ≈25 °C.

Spectroscopic Measurements: A Shimadzu UV-2550 UV–vis spectrophotometer was used to measure steady-state transmittance of substrates and samples. Absorbance was then calculated using the following equation to remove substrate contributions: $\text{Abs} = \log(T_{\text{Substrate}}/T_{\text{Sample}})$, with reflection and scattering effects being ignored.

A Renishaw inVia Raman microscope with a 50× objective in a backscattering configuration was used to collect both PL and Raman spectra. All measurements, unless otherwise stated, were conducted in a nitrogen-purged Linkam sample chamber. All measurements were taken with a defocused laser spot with a radius of ≈10 µm. PL spectra were recorded using 514 nm laser excitation, with no correction being applied for instrument response. Raman spectra were collected at various wavelengths using an argon ion laser (457, 488, and 514 nm), a HeNe laser (633 nm), and a diode laser (785 nm). Acquisition times and laser powers for both PL and Raman measurements were optimized to give the best spectra, but were kept consistent between samples that are compared in the Results and Discussion section. Spectrometer calibration was conducted using a silicon reference sample and background PL was subtracted using a polynomial fit.

In situ photodegradation studies were carried out in both air and nitrogen using the Raman laser excitation source to both degrade the sample and collect Raman or PL spectra simultaneously. Two wavelengths were used for these studies, 633 and 457 nm. The 457 nm laser had an estimated power density at the sample of $\approx 2 \times 10^6$ W m^{-2}, three orders of magnitude larger than 1 sun illumination at 1×10^3 W m^{-2}, allowing for accelerated degradation studies. The approximate power density of the 633 nm laser used for in situ degradation was $\approx 8 \times 10^6$ W m^{-2}, ≈4× that of the 457 nm laser used. Where two different wavelengths have been used for degradation and data collection, Raman or PL spectra were taken in nitrogen, while degradation was conducted in air. The 633 nm excitation was highly resonant with the lower-energy absorption of IDTBR enhancing the PL and Raman intensity of the IDTBR vibrational modes. Due to this, the in situ experiments of the P3HT:IDTBR blend were conducted on the 8 h solar simulator degraded samples that show a quenching of this PL, allowing for Raman spectra collection.

Energetics and Morphology: Ambient photoemission measurements were taken using an APS04 air photoemission system (APS04, by KP Technology) using a 2 mm gold tip under atmospheric conditions. All samples were measured on ITO substrates to ensure proper grounding of the organic thin films. Measurements were taken at multiple positions on the films to ensure reproducibility. The APS data were processed using the protocol described by Baikie et al.[56] This involved taking the cube root of the measured photoemission, fitting the resultant linear region, and extrapolating to zero photoemission to find the HOMO level of the semiconductor. AFM measurements were taken using a Park NX10 AFM system and SmartScan software with Park silicon PPP-NCHR tips.

Computational Methods: DFT calculations were conducted using Gaussian 09 software on the Imperial College High-Performance Computing Service.[57] All simulations have been carried out as single molecules in the gas phase at the B3LYP level of theory with the basis set 6-31G(d,p).[58–61] Alkyl side chains were simplified to methyl groups to reduce computational time and polymers were modeled as pentamers with methyl capping units. Structures were optimized to a local minimum energy conformation with frozen dihedral angles being used to simulate molecular conformational changes. Frequency calculations were carried out to simulate the Raman spectra, and an empirical scaling

factor of 0.97 was used for the frequency of vibration.[62] Visualization of the simulated vibrational modes using GaussView 6.0.16 software was used to aid Raman peak assignment alongside consultation with the literature.[40,41,63,64]

Supporting Information

Supporting Information is available from the Wiley Online Library or from the author.

Acknowledgements

The authors acknowledge the UK EPSRC for the Plastic Electronics Centre for Doctoral Training (EP/L016702/1) funding and CSEM Brasil for studentship. This research was also supported by Global Research Laboratory (GRL) Program through the National Research Foundation of Korea (NRF) funded by the Ministry of Science and ICT (NRF-2017K1A1A2013153). E.M.S., W.C.T., and Z.L. thank the National Research Network in Advanced Engineering Materials (grant number NRN093), the Welsh Assembly Government funded Ser Cymru Solar Project, and UK EPSRC (EP/M025020/1). The authors thank John de Mello and James Bannock of Imperial College London for providing some of the P3HT used, and the Imperial College High-Performance Computing Service for DFT calculations.

Conflict of Interest

The authors declare no conflict of interest.

Keywords

conformational change, nonfullerene acceptor molecular structures, nonfullerene acceptors, organic solar cells, photostability

Received: December 4, 2018
Revised: February 8, 2019
Published online: February 21, 2019

[1] D. Deng, Y. Zhang, J. Zhang, Z. Wang, L. Zhu, J. Fang, B. Xia, Z. Wang, K. Lu, W. Ma, Z. Wei, *Nat. Commun.* **2016**, *7*, 13740.
[2] J. Zhao, Y. Li, G. Yang, K. Jiang, H. Lin, H. Ade, W. Ma, H. Yan, *Nat. Energy* **2016**, *1*, 15027.
[3] C. H. Peters, I. T. Sachs-Quintana, J. P. Kastrop, S. Beaupré, M. Leclerc, M. D. McGehee, *Adv. Energy Mater.* **2011**, *1*, 491.
[4] C. B. Nielsen, S. Holliday, H.-Y. Chen, S. J. Cryer, I. McCulloch, *Acc. Chem. Res.* **2015**, *48*, 2803.
[5] T. Heumueller, W. R. Mateker, A. Distler, U. F. Fritze, R. Cheacharoen, W. H. Nguyen, M. Biele, M. Salvador, M. von Delius, H.-J. Egelhaaf, M. D. McGehee, C. J. Brabec, *Energy Environ. Sci.* **2015**, *9*, 247.
[6] A. Distler, T. Sauermann, H. J. Egelhaaf, S. Rodman, D. Waller, K. S. Cheon, M. Lee, D. M. Guldi, *Adv. Energy Mater.* **2014**, *4*, 1300693.
[7] N. Deb, R. R. Dasari, K. Moudgil, J. L. Hernandez, S. R. Marder, Y. Sun, A. Karim, D. G. Bucknall, *J. Mater. Chem. A* **2015**, *3*, 21856.
[8] B. C. Schroeder, Z. Li, M. A. Brady, G. C. Faria, R. S. Ashraf, C. J. Takacs, J. S. Cowart, D. T. Duong, K. H. Chiu, C. H. Tan, J. T. Cabral, A. Salleo, M. L. Chabinyc, J. R. Durrant, I. McCulloch, *Angew. Chem., Int. Ed.* **2014**, *53*, 12870.
[9] Z. Li, H. C. Wong, Z. Huang, H. Zhong, C. H. Tan, W. C. Tsoi, J. S. Kim, J. R. Durrant, J. T. Cabral, *Nat. Commun.* **2013**, *4*, 2227.
[10] H. K. H. Lee, A. M. Telford, J. A. Röhr, M. F. Wyatt, B. Rice, J. Wu, A. De Castro Maciel, S. M. Tuladhar, E. Speller, J. McGettrick, J. R. Searle, S. Pont, T. Watson, T. Kirchartz, J. R. Durrant, W. C. Tsoi, J. Nelson, Z. Li, *Energy Environ. Sci.* **2018**, *11*, 417.
[11] E. M. Speller, J. D. McGettrick, B. Rice, A. M. Telford, H. K. H. Lee, C. H. Tan, C. S. De Castro, M. L. Davies, T. M. Watson, J. Nelson, J. R. Durrant, Z. Li, W. C. Tsoi, *ACS Appl. Mater. Interfaces* **2017**, *9*, 22739.
[12] W. Zhao, S. Li, H. Yao, S. Zhang, Y. Zhang, B. Yang, J. Hou, *J. Am. Chem. Soc.* **2017**, *139*, 7148.
[13] Z. Fei, F. D. Eisner, X. Jiao, M. Azzouzi, J. A. Röhr, Y. Han, M. Shahid, A. S. R. Chesman, C. D. Easton, C. R. McNeill, T. D. Anthopoulos, J. Nelson, M. Heeney, *Adv. Mater.* **2018**, *30*, 1705209.
[14] N. Gasparini, M. Salvador, S. Strohm, T. Heumueller, I. Levchuk, A. Wadsworth, J. H. Bannock, J. C. de Mello, H.-J. Egelhaaf, D. Baran, I. McCulloch, C. J. Brabec, *Adv. Energy Mater.* **2017**, *7*, 1700770.
[15] H. Cha, J. Wu, A. Wadsworth, J. Nagitta, S. Limbu, S. Pont, Z. Li, J. Searle, M. F. Wyatt, D. Baran, J. S. Kim, I. Mcculloch, J. R. Durrant, *Adv. Mater.* **2017**, *29*, 1701156.
[16] A. Wadsworth, R. S. Ashraf, M. Abdelsamie, S. Pont, M. Little, M. Moser, Z. Hamid, M. Neophytou, W. Zhang, A. Amassian, J. R. Durrant, D. Baran, I. McCulloch, *ACS Energy Lett.* **2017**, *2*, 1494.
[17] Y. Yang, Z. G. Zhang, H. Bin, S. Chen, L. Gao, L. Xue, C. Yang, Y. Li, *J. Am. Chem. Soc.* **2016**, *138*, 15011.
[18] Y. J. Hwang, H. Li, B. A. E. Courtright, S. Subramaniyan, S. A. Jenekhe, *Adv. Mater.* **2016**, *28*, 124.
[19] S. Holliday, R. S. Ashraf, C. B. Nielsen, M. Kirkus, J. A. Röhr, C. H. Tan, E. Collado-Fregoso, A. C. Knall, J. R. Durrant, J. Nelson, I. McCulloch, *J. Am. Chem. Soc.* **2015**, *137*, 898.
[20] S. Holliday, R. S. Ashraf, A. Wadsworth, D. Baran, S. A. Yousaf, C. B. Nielsen, C.-H. Tan, S. D. Dimitrov, Z. Shang, N. Gasparini, M. Alamoudi, F. Laquai, C. J. Brabec, A. Salleo, J. R. Durrant, I. McCulloch, *Nat. Commun.* **2016**, *7*, 11585.
[21] J. Razzell-Hollis, W. C. Tsoi, J.-S. Kim, *J. Mater. Chem. C* **2013**, *1*, 6235.
[22] W. Zhang, Z. Mao, N. Zheng, J. Zou, L. Wang, C. Wei, J. Huang, D. Gao, G. Yu, *J. Mater. Chem. C* **2016**, *4*, 9266.
[23] S. Wood, J. H. S. Kim, D. H. Hwang, J. H. S. Kim, *Chem. Mater.* **2015**, *27*, 4196.
[24] H. Huang, L. Yang, A. Facchetti, T. J. Marks, *Chem. Rev.* **2017**, *117*, 10291.
[25] A. Mahmood, A. Tang, X. Wang, E. Zhou, *Phys. Chem. Chem. Phys.* **2019**, *21*, 2128.
[26] J. Wu, Y. Xu, Z. Yang, Y. Chen, X. Sui, L. Yang, P. Ye, T. Zhu, X. Wu, X. Liu, H. Cao, A. Peng, H. Huang, *Adv. Energy Mater.* **2019**, *9*, 1803012.
[27] Y. Liu, Z. Zhang, S. Feng, M. Li, L. Wu, R. Hou, X. Xu, X. Chen, Z. Bo, *J. Am. Chem. Soc.* **2017**, *139*, 3356.
[28] Z. Zhang, J. Yu, X. Yin, Z. Hu, Y. Jiang, J. Sun, J. Zhou, F. Zhang, T. P. Russell, F. Liu, W. Tang, *Adv. Funct. Mater.* **2018**, *28*, 1705095.
[29] D. Baran, R. A. S. Ashraf, D. A. Hanifi, M. Abdelsamie, N. Gasparini, J. A. Röhr, S. Holliday, A. Wadsworth, S. Lockett, M. Neophytou, C. J. M. Emmott, J. Nelson, C. J. Brabec, A. Amassian, T. Kirchartz, J. R. Durrant, I. Mcculloch, D. Baran, R. A. S. Ashraf, S. Holliday, A. Wadsworth, S. Lockett, P. J. R. Durrant, *Nat. Mater.* **2016**, *16*, 363.
[30] W. Zhao, D. Qian, S. Zhang, S. Li, O. Inganäs, F. Gao, J. Hou, *Adv. Mater.* **2016**, *28*, 4734.
[31] Z. Li, K. Jiang, G. Yang, J. Y. L. Lai, T. Ma, J. Zhao, W. Ma, H. Yan, *Nat. Commun.* **2016**, *7*, 13094.

[32] F. Zhao, S. Dai, Y. Wu, Q. Zhang, J. Wang, L. Jiang, Q. Ling, Z. Wei, W. Ma, W. You, C. Wang, X. Zhan, *Adv. Mater.* **2017**, *29*, 1700144.
[33] A. Wadsworth, Z. Hamid, M. Bidwell, R. S. Ashraf, J. Khan, C. Cendra, J. Yan, E. R. Soltani, A. A. Y. Guilbert, A. Salleo, J. Nelson, F. Laquai, I. Mcculloch, *Adv. Energy Mater.* **2018**, *8*, 1801001.
[34] J. Razzell-Hollis, S. Limbu, J. S. Kim, *J. Phys. Chem. C* **2016**, *120*, 10806.
[35] W. C. Tsoi, D. T. James, J. S. Kim, P. G. Nicholson, C. E. Murphy, D. D. C. Bradley, J. Nelson, J. S. Kim, *J. Am. Chem. Soc.* **2011**, *133*, 9834.
[36] S. Wood, J. R. Hollis, J.-S. S. Kim, *J. Phys. D: Appl. Phys.* **2017**, *50*, 073001.
[37] J. Razzell-Hollis, J. Wade, W. C. Tsoi, Y. Soon, J. Durrant, J.-S. Kim, *J. Mater. Chem. A* **2014**, *2*, 20189.
[38] S. Wood, J. Wade, M. Shahid, E. Collado-Fregoso, D. D. C. Bradley, J. R. Durrant, M. Heeney, J.-S. Kim, *Energy Environ. Sci.* **2015**, *8*, 3222.
[39] M. J. Newman, E. M. Speller, J. Barbé, J. Luke, M. Li, Z. Li, Z. K. Wang, S. M. Jain, J. S. Kim, H. K. H. Lee, W. C. Tsoi, *Sci. Technol. Adv. Mater.* **2018**, *19*, 194.
[40] J. P. Schmidtke, J. S. Kim, J. Gierschner, C. Silva, R. H. Friend, *Phys. Rev. Lett.* **2007**, *99*, 167401.
[41] D. Venkateshvaran, M. Nikolka, A. Sadhanala, V. Lemaur, M. Zelazny, M. Kepa, M. Hurhangee, A. J. Kronemeijer, V. Pecunia, I. Nasrallah, I. Romanov, K. Broch, I. McCulloch, D. Emin, Y. Olivier, J. Cornil, D. Beljonne, H. Sirringhaus, *Nature* **2014**, *515*, 384.
[42] K. G. Jespersen, W. J. D. Beenken, Y. Zaushitsyn, A. Yartsev, M. Andersson, T. Pullerits, V. Sundström, *J. Chem. Phys.* **2004**, *121*, 12613.
[43] M. S. Vezie, S. Few, I. Meager, G. Pieridou, B. Dörling, R. S. Ashraf, A. R. Goñi, H. Bronstein, I. McCulloch, S. C. Hayes, M. Campoy-Quiles, J. Nelson, *Nat. Mater.* **2016**, *15*, 746.
[44] S. Scholz, D. Kondakov, B. Lüssem, K. Leo, *Chem. Rev.* **2015**, *115*, 8449.
[45] W. Song, J. Y. Lee, *Adv. Opt. Mater.* **2017**, *5*, 1600901.
[46] M. Nikolka, I. Nasrallah, B. Rose, M. K. Ravva, K. Broch, A. Sadhanala, D. Harkin, J. Charmet, M. Hurhangee, A. Brown, S. Illig, P. Too, J. Jongman, I. McCulloch, J. L. Bredas, H. Sirringhaus, *Nat. Mater.* **2017**, *16*, 356.
[47] M. Manceau, A. Rivaton, J. L. Gardette, S. Guillerez, N. Lemaître, *Polym. Degrad. Stab.* **2009**, *94*, 898.
[48] M. Manceau, J. Gaume, A. Rivaton, J. L. Gardette, G. Monier, L. Bideux, *Thin Solid Films* **2010**, *518*, 7113.
[49] J. Ficker, H. Von Seggern, H. Rost, W. Fix, W. Clemens, I. McCulloch, *Appl. Phys. Lett.* **2004**, *85*, 1377.
[50] W. C. Tsoi, S. J. Spencer, L. Yang, A. M. Ballantyne, P. G. Nicholson, A. Turnbull, A. G. Shard, C. E. Murphy, D. D. C. Bradley, J. Nelson, J. S. Kim, *Macromolecules* **2011**, *44*, 2944.
[51] G. M. Paternò, V. Robbiano, K. J. Fraser, C. Frost, V. Garciá Sakai, F. Cacialli, V. García Sakai, F. Cacialli, *Sci. Rep.* **2017**, *7*, 41013.
[52] S. Bellani, D. Fazzi, P. Bruno, E. Giussani, E. V. Canesi, G. Lanzani, M. R. Antognazza, *J. Phys. Chem. C* **2014**, *118*, 6291.
[53] E. A. Bazzaoui, G. Lévi, S. Aeiyach, J. Aubard, J. P. Marsault, P. C. Lacaze, *J. Phys. Chem.* **1995**, *99*, 6628.
[54] M. Baibarac, M. Lapkowski, A. Pron, S. Lefrant, I. Baltog, *J. Raman Spectrosc.* **1998**, *29*, 825.
[55] E. Alveroglu, *J. Mol. Struct.* **2015**, *1086*, 86.
[56] I. D. Baikie, A. C. Grain, J. Sutherland, J. Law, *Energy Procedia* **2014**, *60*, 48.
[57] M. J. Frisch, G. W. Trucks, H. B. Schlegel, G. E. Scuseria, M. A. Robb, J. Cheeseman, G. Scalmani, V. Barone, B. Mennucci, G. A. Petersson, H. Nakatsuji, M. Caricato, X. Li, H. P. Hratchian, A. F. Izmaylov, J. Bloino, G. Zheng, J. L. Sonnenberg, M. Hada, M. Ehara, K. Toyota, R. Fukuda, J. Hasegawa, M. Ishida, T. Nakajima, Y. Honda, O. Kitao, H. Nakai, T. Vreven, J. A. Montgomery Jr., J. E. Peralta, F. Ogliaro, M. Bearpark, J. J. Heyd, E. Brothers, K. N. Kudin, V. N. Staroverov, R. Kobayashi, J. Normand, K. Raghavachari, A. Rendell, J. C. Burant, S. S. Iyengar, J. Tomasi, M. Cossi, N. Rega, J. M. Millam, M. Klene, J. E. Knox, J. B. Cross, V. Bakken, C. Adamo, J. Jaramillo, R. Gomperts, R. E. Stratmann, O. Yazyev, A. J. Austin, R. Cammi, C. Pomelli, J. W. Ochterski, R. L. Martin, K. Morokuma, V. G. Zakrzewski, G. A. Voth, P. Salvador, J. J. Dannenberg, S. Dapprich, A. D. Daniels, O. Farkas, J. B. Foresman, J. V. Ortiz, J. Cioslowski, D. J. Fox, *Gaussian 09, Revision A.1*, Gaussian, Inc., Wallingford, CT **2009**.
[58] A. D. Becke, *J. Chem. Phys.* **1993**, *98*, 5648.
[59] G. A. Petersson, M. A. Al-Laham, *J. Chem. Phys.* **1991**, *94*, 6081.
[60] G. A. Petersson, A. Bennett, T. G. Tensfeldt, M. A. Al-Laham, W. A. Shirley, J. Mantzaris, *J. Chem. Phys.* **1988**, *89*, 2193.
[61] P. J. Stephens, F. J. Devlin, C. F. Chabalowski, M. J. Frisch, *J. Phys. Chem.* **1994**, *98*, 11623.
[62] M. L. Laury, M. J. Carlson, A. K. Wilson, *J. Comput. Chem.* **2012**, *33*, 2380.
[63] S. Wood, J.-S. S. J. S. Kim, D. T. James, W. C. Tsoi, C. E. Murphy, J.-S. S. J. S. Kim, *J. Chem. Phys.* **2013**, *139*, 064901.
[64] X. Rodriguez-Martinez, M. S. Vezie, X. Shi, I. McCulloch, J. Nelson, A. R. Goñi, M. Campoy-Quiles, *J. Mater. Chem. C* **2017**, *5*, 7270.